DOI: 10.15480/882.9332

Eighth International Symposium on Marine Propulsors
smp'24, Berlin, Germany, March 2024

A Numerical Study on Model Propeller Performance Prediction Including Transitional and Passively Controlled Boundary Layer Considerations

Maarten Kerkvliet[1], João Baltazar[2], Bart Schuiling[1], Luís Eça[2]

[1]Maritime Research Institute Netherlands (MARIN), Wageningen, The Netherlands
[2]Instituto Superior Técnico (IST, ULisboa), Lisboa, Portugal

ABSTRACT

Viscous flow simulations, utilising Computational Fluid Dynamics (CFD), have increasingly become the standard approach in the design and optimisation processes for predicting propeller performance. This is primarily due to the significant influence of viscous effects on propeller performance, encompassing phenomena such as tip and hub vortices, tip vortex cavitation inception, flow separation, and the transition from laminar to turbulent boundary layers at model-scale. Numerous studies have demonstrated the necessity of incorporating transition modelling in CFD to accurately determine propeller performance at model-scale, whereas full-scale simulations can successfully rely on two-equation turbulence models.

However, despite these advancements in CFD, the industry continues to rely on a relatively simplistic procedures to scale model test results to full-scale in order to predict ship propeller performance. Generally, the conventional scaling procedures focus solely on reducing sectional drag between the model and full-scale propeller, assuming a partially laminar boundary layer at model-scale. Nevertheless, it is important to recognize that this approach oversimplifies the discrepancies between laminar and turbulent propeller boundary layers.

Therefore, the aim of this paper is to demonstrate that CFD, when employing the appropriate turbulence and transition models, can accurately predict propeller performance at model-scale, in scenarios involving partially laminar or fully turbulent boundary layers. Consequently, the findings provide additional insights on improving extrapolation methods through CFD simulations, particularly when model-scale considerations prioritize the accurate development of turbulent boundary layers.

A Reynolds averaged Navier-Stokes solver (RANS) was used in combination with the k-ω SST turbulence and γ-Re_θ transition model for a modern designed MARIN stock propeller. The CFD results were compared to Experimental Fluid Dynamics (EFD) results, which involved propellers equipped with and without innovative turbulence stimulators, also known as turbulators. In addition to comparing performance characteristics, the boundary layer flows regimes were also examined using EFD paint test results. Furthermore, full-scale Reynolds CFD simulations were conducted and compared to conventionally extrapolated EFD results.

Excellent comparisons were achieved between EFD and CFD for model-scale Reynolds numbers, encompassing both uncontrolled and passively controlled boundary layers. A clear trend of Reynolds scaling was observed for propellers with a turbulent boundary layer at model-scale. However, this trend was not evident for propellers with laminar or partially laminar boundary layers at model-scale, demonstrating that the relevant boundary layer regimes should be modelled correctly.

Keywords

Propeller Performance; Transition Model; Turbulence Stimulation; Paint Tests; Full Scale.

1 INTRODUCTION

The prediction of propeller performance is a critical task in the design and optimization of marine propulsion systems. It involves the estimation of propeller thrust, torque, efficiency, and other hydrodynamic characteristics across a wide range of operational conditions, which depends on various factors such as propeller geometry, inflow velocity, cavitation, and Reynolds number. Model-scale experiments frequently serve as the foundation for this type of research, complemented by extrapolation methods to predict the propeller performance at full-scale.

Challenges in predicting propeller performance at model-scale are as old as the model basins themselves. In general, all model-scale experiments are inevitably associated with Reynolds number scaling effects, particularly when considering the presence of a laminar or transitional boundary layer at model-scale, in contrast to the fully turbulent boundary layer at the full scale. These scaling problems were affirmed by the findings of the Propeller Committee of the ITTC as documented by Allan et al. (1951). A comprehensive review of the literature on this topic is provided by Schuiling et al. (2024).

In general, a turbulent boundary layer significantly reduces the performance characteristics of the propeller, in terms of thrust reduction and increased torque. Conversely, a laminar boundary layer at model-scale is prone to separation under adverse pressure gradients, which as a result also reduces the sectional lift and increases the pressure drag. Additionally, it is important to note that the occurrence of flow separation is closely related to propeller design and operational condition. Some of these issues were addressed by the Powering Performance Committee in the report of the ITTC-1978 procedure (Aucher et al. 1978), where it was reported that laminar flow exists over the propeller blades in standard open-water tests and cover up to approximately 40% of the blade section chord. According to Fagerjord and Andersen (1982) conditions to obtain fully turbulent flow may require Reynolds numbers larger than $5 \cdot 10^6$, which means an increased propeller diameter and propeller rotation rate, but this is very difficult to achieve with standard model-scale experimental techniques. An alternative approach involves using turbulence stimulators like sand-grain strips or studs near the leading edge of the blade, a concept explored by researchers such as Tamura and Sasajima (1977). Additionally, Kuiper (1981) and Boorsma (2000) conducted a thorough study, including leading edge roughness, on the visualization of the boundary layer regimes by paint test experiments. Also Jessup (1989) analysed detailed Laser Doppler Velocimetry (LDV) measurements of the velocity profiles for smooth and tripped propeller blades. The main conclusion from these studies was that the boundary layer flow on the outer radii can be easily tripped to turbulence using leading edge roughness, and that the extrapolation of model propeller performance to full-scale performance could be improved by using leading edge roughness to control the regime of the boundary layer. However, they also found some unexpected results and the lack of precision and accuracy of computational tools did not allow them to figure this out in detail. Furthermore, it proved challenging to apply them in a well-controlled manner without changing the local geometry and reliable scale effect corrections were required. Moreover, as stated in the ITTC-87 (1987) report, there is also the challenging aspect to convince propeller designers, ship owners, and builders that intentionally introducing a purposeful efficiency loss of several percent at the model-scale is the correct approach for making precise predictions regarding the efficiency of the full-scale propeller. Due to these considerations, the utilization of turbulence tripping was not advisable at that time for model-scale testing, even though it could potentially serve as a valuable tool for evaluating and understanding the impact of variations in flow regime on model-scale propeller performance.

To improve the accuracy of propeller performance prediction, several Computational Fluid Dynamics (CFD) methods have been developed that incorporate transition-sensitive turbulence models. These models are able to capture the onset and extent of transition, as well as the resulting changes in skin-friction, pressure distribution, and wake formation. This resulted in subsequent experiments that included paint tests, alongside numerical simulations carried out by various institutes. Notably, Hasuike et al. (2017) conducted an extensive study examining propeller boundary layers on small blade area propellers. They employed a combination of experimental paint tests and numerical analyses in their investigation. The CFD simulations incorporate transition modelling to ensure high modelling accuracy. The findings indicated that, in both open-water tests and self-propulsion tests, the predominant nature of the boundary layer was laminar, leading to the observation of extensive laminar flow separation regions near the trailing edge. The authors emphasized the importance of integrating numerical tools to achieve more reliable propeller performance results and the need to make an improvement on the scaling procedure for accurate extrapolation to full-scale conditions. Lücke (2019) reported similar observations of boundary layer flow regimes through propeller paint tests and a CFD study, examining the flow behaviour for various propeller designs. The CFD study included a comparative analysis of fully turbulent and fully laminar flows, excluding the use of a transition model. On this basis, he concluded that it is crucial to model the accurate combination of laminar and turbulent boundary layer regimes. This is essential because the experimental results differ from the results of simplified assumptions that consider only one of the two regimes.

Moreover, Rijpkema et al. (2015) and Baltazar et al. (2021) showed a detailed analysis of Reynolds number effect for propeller performance predictions in open-water conditions ranging from laminar flow ($Re = 10^4$) up to full-scale ($Re = 10^7$) Reynolds numbers. Even though this study of Baltazar et al. (2021) incorporated transition modelling, a comparison with model-scale experimental results reveals significant comparison errors, particularly for advance ratios near the design condition. Considering that the flow over the propeller blade at model-scale Reynolds numbers predominantly exists in the critical Reynolds number regime, where the transition from laminar to turbulent flow occurs, it is likely that the disparities in performance are associated with the transition from laminar to turbulent flow on the propeller blade. Contrarily, the standard k-ω Shear-Stress Transport (SST) model totally fails to accurately predict laminar-to-turbulence transition, consistently showing an early transition with a limited transition length, as noted by Eça and Hoekstra (2008), Rijpkema et al. (2015) and Lopes (2021).

Furthermore, Li et al. (2019) presented findings from open-water tests conducted on three propeller designs at both low and high model-scale Reynolds numbers. They compared experimental results, incorporating paint tests, with numerical results obtained using the Local Correlation Transition Model (LCTM) γ transition model. At low Reynolds numbers, typical of the propeller's conditions in self-propulsion tests (SPT), laminar flow predominated for all propellers, with observed separated flow near the trailing edge. Conversely, at higher Reynolds numbers as commonly used in propeller open-water tests (POT), a mix of laminar, transitional, and turbulent flow was identified. Consequently, extrapolating the results from model-scale conditions to

full-scale predictions is highly depended on the conditions tested in SPT and POT. To address this, the authors propose a 2POT procedure, involving two open-water tests. The first is conducted at a low Reynolds number equivalent to that in self-propulsion tests, facilitating the analysis of SPT results. The second, at a higher Reynolds number, is used to extrapolate open-water characteristics to full-scale based on the ITTC-78 scaling procedure.

Similarly, Grlj et al. (2022) studied scale effects on the open-water propeller performance for Reynolds numbers ranging from $1.3 \cdot 10^6$ to $3.3 \cdot 10^8$. They compared experimental model-scale results with numerical results using the k-ω SST turbulence model combined with and without the LCTM γ-Re_θ transition model. From the results, it was concluded that the scale effects on open-water characteristics were significantly lower when the transition model was applied, but the extrapolated model-scale values of the open-water efficiency, using the ITTC 1978 performance prediction method, still remains too low compared to results obtained by full-scale simulations.

The analysis of the sensitivity of inflow boundary conditions has been conducted for various canonical cases by Lopes (2021). Furthermore, Katsuno et al. (2021), Gaggero (2022) and Baltazar et al. (2018, 2023) have studied this sensitivity concerning open-water propeller performance. Gaggero (2022) reported a good comparison agreement between CFD and EFD results for a conventional and an unconventional propeller design. This agreement was achieved solely when employing the transition-sensitive turbulence model LCTM γ-Re_θ, alongside adjusting turbulence parameters at the domain inlet to achieve a reference turbulence intensity of 1% at the propeller plane. In the work of Baltazar et al. (2023), the inlet turbulence quantities are chosen to qualitatively match the experimental transition location obtained from paint test photographs. This study illustrates the limitations in the predictive capabilities of the γ-Re_θ turbulent-transition model due to this strong dependence of the inlet turbulence quantities on the predicted performance. An important note is that the inlet turbulence quantities may not be realistic from a physics point of view, but depend on the Reynolds number and the propeller loading condition.

Another improvement of the modelling of these flow complexity within model-scale rotating propellers could be accomplished by integrating cross-flow as a transition mechanism, as studied by Moran-Guerrero et al. (2018) and Lopes et al. (2023). These studies show the potential improvement of model-scale performance prediction by including cross-flow modelling. However, the added value remains unclear at this point, primarily because there is a deficiency in direct comparisons with paint tests.

While there has been notable advancement in transition models, their high sensitivity poses a limitation to their applicability. And despite numerical predictions frequently aligning with propeller performance observed in model tests, regularly unexpected differences between experimental and numerical performance predictions are found. Additionally, the challenge persists in the extrapolation process, which currently relies on assuming partial laminar flow rather than accounting for full-scale conditions, thereby introducing complications in the extrapolation. In an effort to deviate from the established pattern, MARIN conducted a comprehensive series of paint tests on various stock propellers, subjecting them to assessments both in the presence and absence of turbulence stimulation. The detailed findings of this extensive experimental study including high quality boundary layer visualisation by performing paint-tests and an innovative method to stimulate turbulence in an efficient and controllable way is reported by Schuiling et al. (2024).

This paper focuses on a comparative analysis between experimental results obtained with uncontrolled and passively controlled boundary layers and those derived from CFD. The CFD considers scenarios both with and without the inclusion of transition modelling. These advancements in experimental and numerical techniques are expected to yield more consistent model test results and enhance the reliability of extrapolation predictions.

2 METHODOLOGY

2.1 ReFRESCO

ReFRESCO (www.marin.nl) is a CFD software package, developed at the Maritime Research Institute Netherlands (MARIN) in collaboration with several universities and partners. It solves unsteady (in)compressible viscous flows based on the Navier-Stokes equations, complemented with turbulence models and volume-fraction transport equations for different phases. The equations are discretized using a finite-volume approach of the continuity and momentum equations written in conservative integral form. The solver uses a collocated, cell-centred variable arrangement and a face-based approach that enables the use of unstructured, body-fitted computational meshes with arbitrary polyhedral cells. Picard linearisation is applied and segregated or coupled approaches are available with mass conservation ensured using a SIMPLE-like algorithm and a pressure-weighted interpolation technique to avoid spurious oscillations. For turbulence modelling different turbulence models are available depending on the application at hand. Mesh handling techniques such as moving, sliding, deforming and overset-meshes are available, as well as automatic mesh refinement and coarsening. The six-DoF rigid-body motion is being solved within the code and full fluid-structure interaction (FSI) with flexible-body motion is also possible. Lastly, coupling to external codes is made possible for propeller models (RANS-BEM coupling), fast-time simulation tools (MARIN's time-domain simulation framework XMF) and wave generation potential flow codes (OceanWave3D, SWASH, REEF3D). Thorough code verification is performed for all releases of ReFRESCO.

2.2 Turbulence and transition models

This study includes only one turbulence model and one transition model, both selected from prior research within this specific field of turbulence and transition modelling (e.g. Eça et al. 2023a, Baltazar et al. 2023, Lopes et al. 2022).

The turbulence model employed in this study is the well-known k-ω SST two-equation eddy-viscosity model developed by Menter et al. (2003). This model is based on a blend between the k-ω and k-ϵ turbulence models to combine the best properties of both models and is therefore a popular choice of turbulence model for many maritime engineering applications. Details on the transport equations, model constants, blending and damping functions are given in Menter et al. (2003).

This turbulence model can be combined with the γ-Re_θ LCTM transition model as developed by Langtry and Menter (2009), which is also incorporated in this study. This transition model includes two additional transport equations, one for the intermittency γ and the second one for the transition onset momentum-thickness Reynolds number $\tilde{Re}_{\theta t}$.

The integration of the transition model with the k-ω SST turbulence model involves adjusting the production (P_k) and dissipation (D_k) terms in the turbulence kinetic energy transport equation. The terms of the SST turbulence model are given by

$$\begin{aligned} P_{k,SST} &= \min\left(\mu_t S^2, 10 D_k\right), \\ D_{k,SST} &= \beta^* \rho k \omega. \end{aligned} \tag{1}$$

The transition model calculates an effective intermittency denoted as γ_{eff}, incorporating an additional formulation γ_{sep} to handle separation induced transition. The change of the production and dissipation terms incorporating γ_{eff} becomes

$$\begin{aligned} P_k &= \gamma_{\text{eff}} P_{k,SST}, \\ D_k &= \min(\max(\gamma_{\text{eff}}, 0.1), 1.0) D_{k,SST}. \end{aligned} \tag{2}$$

Suppressing the production of turbulent kinetic energy results in the development of a laminar boundary layer, until a critical Reynolds number $Re_{\theta c}$ which dictates the start of transition by increasing the intermittency to one. From that location a fully turbulent boundary layer will be obtained. The length of the transition region and the transition onset location are defined by empirical correlations.

2.3 Propeller geometry

A modern designed MARIN stock propeller was considered for the present study. In the publication by Schuiling et al. (2024), this propeller is identified as *Propeller-B*. The main propeller particulars are listed in Table 1. The diameter D in millimetres, dimensionless chord length $c_{0.7R}/D$ and pitch ratio $P/D(0.7R)$ at radii $r = 0.7R$, with R being the propeller radius. Furthermore the blade-area ratio is designated by A_e/A_o and the number of blades by Z.

Table 1: Characteristics of the test-case propeller

Propeller	Diameter	D	300 mm
	Number of blades	Z	5
	Chord at 0.7R	$c_{0.7R}/D$	0.279
	Pitch	$P_{0.7R}$/D	1.045
	Expanded Area Ratio	A_e/A_o	0.636

The propeller operating conditions are defined by the advance condition and the characteristic propeller Reynolds number given by

$$J = \frac{V_a}{nD}, \tag{3}$$

$$Re = \frac{\rho\, c_{0.7R}\, V_{0.7R}}{\mu}. \tag{4}$$

Here, V_a is the propeller advance speed, ρ the density and μ the dynamic viscosity of the fluid. It is common to define the dimensionless propeller characteristic at $r/R = 0.7$, therefore the reference velocity for the Reynolds number is defined by

$$V_{0.7R} = \sqrt{V_a^2 + (0.7\,\pi\,n\,D)^2}. \tag{5}$$

The open-water characteristics are quantified using the thrust coefficient (K_T), the torque coefficient (K_Q), and the open-water efficiency (η_o). These are defined by the respective formulas:

$$K_T = \frac{T}{\rho n^2 D^4}, \tag{6}$$

$$K_Q = \frac{Q}{\rho n^2 D^5}, \tag{7}$$

$$\eta_o = \frac{J K_T}{2\pi K_Q}. \tag{8}$$

Here, T and Q are the obtained propeller thrust and torque, respectively.

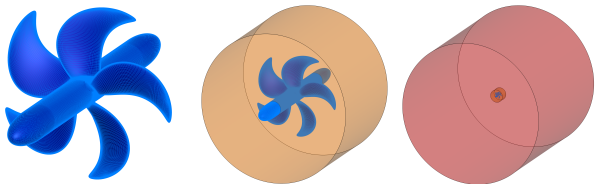

Figure 1: Example of the surface grid, inner and outer domains

2.4 Numerical setup

All simulations were performed using the frozen rotor approach combined with non-conformal interfaces. This means that only the inner-domain is solved by using the absolute velocity formulation where the equations are solved in the rotational reference frame, but written in the earth-fixed reference frame.

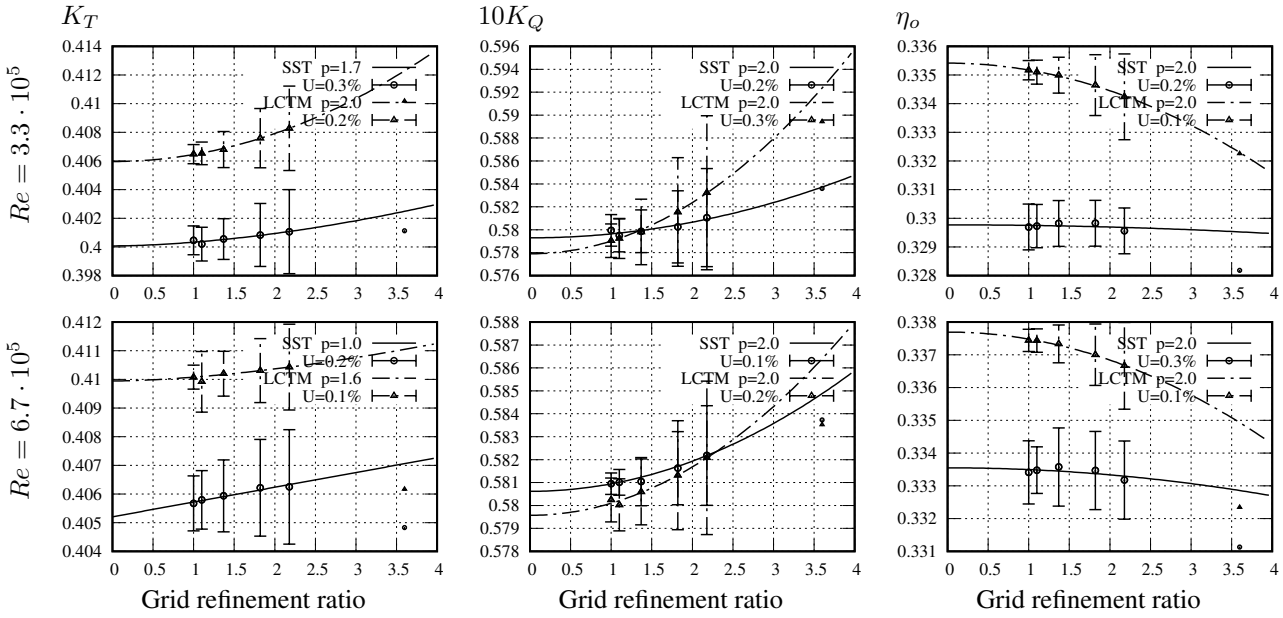

Figure 2: Estimated numerical uncertainty based on grid refinement for model-scale Reynolds numbers at high loading condition $J = 0.3$

Table 2: Grid information showing grid refinement ratio r_i, total number of cells N_{cells}, number of faces on a single blade surface N_{faces} and the average distance in wall coordinates y^+

Grid	r_i	N_{cells}	N_{faces}	y^+
G1	1.0	101,498,180	74,140	0.37
G2	1.1	76,869,152	61,360	0.42
G3	1.4	40,691,006	39,424	0.51
G4	1.8	18,004,238	22,320	0.68
G5	2.2	10,905,730	15,580	0.83
G6	3.6	2,819,196	5,724	1.43
FS	-	25,756,766	28,272	0.1

In order to analyse the numerical uncertainty, a set of nearly-geometrically similar grids was generated for this propeller. The numerical domain is divided into two cylindrical shaped sub-domains, as illustrated by Figure 1. The inner domain is a multi block-structured (GridPro) grid in the vicinity of the propeller, with a diameter and total length of 3.5 and 2.5 times the propeller diameter (D), respectively. The outer domain is an unstructured (Hexpress) grid with both diameter and total length equal to 20D.

For the model-scale Reynolds numbers the grids range from approximately 3 to 100 million cells, indicated by G6 to G1, respectively. More details are given in Table 2, including the grid refinement ratio r_i, the number of faces on a single blade surface N_{faces}, and the average of the dimensionless distance in wall coordinates y^+. These averaged values correspond to the simulations using the k-ω SST turbulence model at the design advance condition for the high model-scale Reynolds number of $7 \cdot 10^5$.

For the full-scale simulations the same grid topology is used, but the wall-normal refinement is adapted from model-scale to full-scale Reynolds numbers, to ensure $y+ < 1$ for all Reynolds number regimes. Therefore, the boundary-layer is fully resolved and no wall functions are used. The full-scale grid is indicated by FS in Table 2. The averaged $y+$ value corresponds to the simulation at the design condition based on a full-scale Reynolds number of $1 \cdot 10^7$.

3 RESULTS

3.1 Numerical uncertainty estimation

Prior to the comparison of the model-scale RANS predictions with the experimental data, a thorough examination of the numerical uncertainties inherent in the simulations is performed for this propeller, which involved the results of the open-water performance in terms of thrust coefficient (K_T), torque coefficient (K_Q) and efficiency coefficient (η_o).

The main goal of the solution verification exercises is to check the consistency of the results obtained by the k-ω SST model without and with the γ-Re_θ LCTM transition model. This provides useful information about the turbulence modelling performance. The validation exercises are not performed strictly in compliance with the ASME V&V20 Standard (ASME 2009) due to the lack of the experimental uncertainties for these quantities. Nonetheless, the comparison with the results offers a quantitative analysis. Although the numerical analysis covers the entire range of advance conditions $0.3 > J > 1.05$, our focus in this context will be towards the examination of two separate conditions: a high loading condition ($J = 0.3$) and the design point ($J = 0.8$). The conclusions drawn from these conditions represent all advance conditions inbetween. The propeller rotation rates vary from $n = 400$ to 800 rpm, corresponding to a Reynolds number range ($Re_{0.7R}$) from $3.3 \cdot 10^5$ to $7.0 \cdot 10^5$. A summary of these conditions is presented in Table 3.

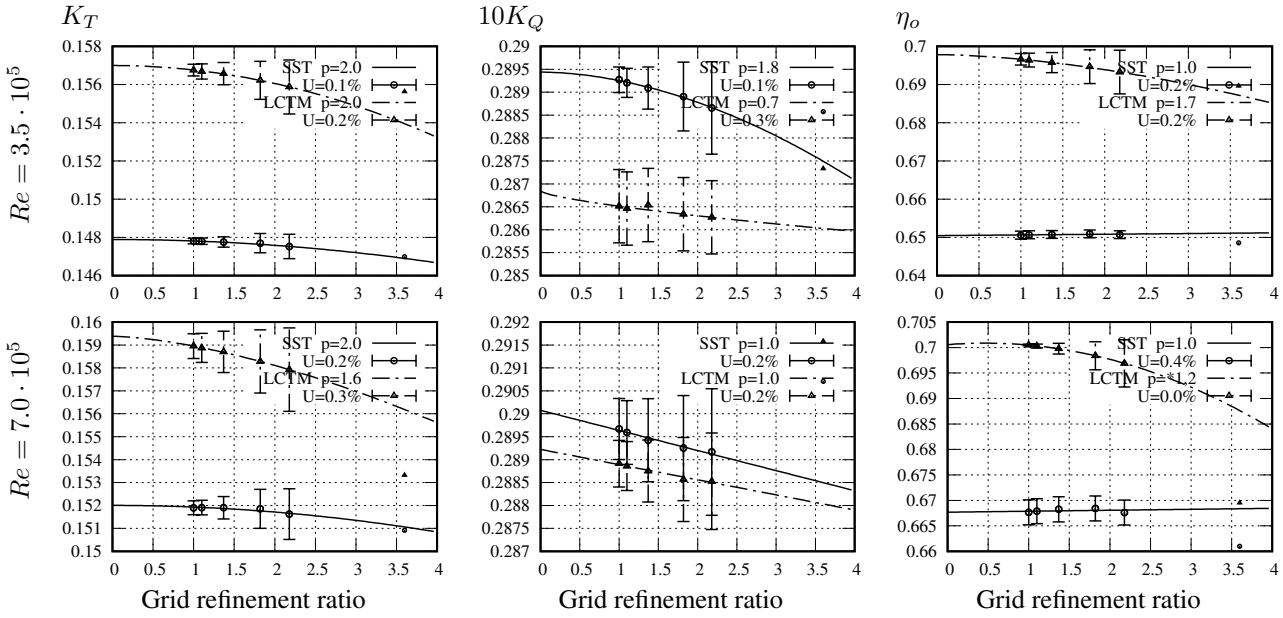

Figure 3: Estimated numerical uncertainty based on grid refinement for model-scale Reynolds numbers at high loading condition $J = 0.8$

Table 3: Operating conditions for the numerical uncertainty estimation

Propeller Conditions		Reynolds Numbers low Re	high Re
J=0.3	Re [-]	$3.3 \cdot 10^5$	$6.7 \cdot 10^5$
	V_a [m/s]	0.6	1.2
	n [rpm]	400	800
J=0.8	Re [-]	$3.5 \cdot 10^5$	$7.0 \cdot 10^5$
	V_a [m/s]	1.6	3.2
	n [rpm]	400	800

The numerical uncertainties are estimated for all quantities of interest using the numerical uncertainty procedure as proposed in Eça and Hoekstra (2014), which is based on spatial grid refinement. The grid refinement ratio, or relative step size, is indicated by r_i in Table 2 is defined by

$$r_i = \frac{h_i}{h_1} = \left(\frac{(N_1)_{\text{cells}}}{(N_i)_{\text{cells}}}\right)^{1/3} = \left(\frac{(N_1)_{\text{faces}}}{(N_i)_{\text{faces}}}\right)^{1/2}. \quad (9)$$

Given that the grids comprise both a multi-block structured propeller grid and an unstructured grid for the outer domain, determining the grid refinement ratio is best achieved by evaluating either the cell count of the multi-block structured grid or the number of faces on a single blade. This is due to the challenging nature of precisely controlling the refinement areas of the unstructured grid of the outer domain.

All simulations were executed in double-precision, thereby assuming that the impact of round-off errors on numerical uncertainty is negligible. The iterative convergence criteria required an L2 value for the normalized residual of all transport equations below 10^{-6}. This criterion ensures that the primary source of numerical uncertainty is the contribution from the discretisation error.

The basics of the estimation of the discretisation error starts with a power series expansion of a quantity of interest Φ as a function of the grid refinement ratio r_i.

$$\Phi_i = \Phi_0 + \alpha r_i^{p_x} \quad (10)$$

Where Φ_0 is the estimate of the exact solution, α is a constant related to the grid and p_x is the observed order of grid convergence. Equation 10 is solved in the least-squares sense and alternative power series expansions with fixed exponents are used if there is anomalous behaviour, i.e. apparent non-monotonic convergence or unreliable values of p_x. In any case, the discretisation error ϵ is obtained from

$$\epsilon = \Phi_i - \Phi_0 \quad (11)$$

and the numerical uncertainty U_{num} is determined by

$$U_{\text{num}} = F_s|\epsilon|, \quad (12)$$

where F_s represents a safety factor that depends on the standard deviation of the least-squares fit. A comprehensive explanation of the methodology, along with example results, is provided in Eça et al. (2023c).

The estimated numerical uncertainty for the coefficients K_T, K_Q and η_o, at the advance conditions $J = 0.3$ and $J = 0.8$, are presented in Figure 2 and Figure 3. Both figures contain six plots of the CFD results by employing either the LCTM γ-Re_θ transition model or the k-ω SST turbulence model. The top row represents the low Reynolds number, while the higher Reynolds number is given in the bottom row. The fits that estimate the exact solution of the

quantities of interest are based on the data of the five finest grids, leaving out the coarsest grid ($r_i = 3.6$) results. The results are presented using symbols and error bars, with the legend specifying the uncertainty (U) of the finest grid and indicating the order of the fit (p).

In general, it can be concluded that the results obtained with the LCTM γ-Re_θ transition model exhibit a more pronounced influence from spatial resolution. This can be attributed to the transition from laminar to a turbulent boundary layer, indicating that the resolution in the flow direction is highly sensitive to such changes. Nevertheless, the majority of the results exhibit a consistent convergence toward the results obtained with the fine grid, displaying either a monotonic trend or, in some cases, a linear fit. The numerical uncertainties are minimal, with $U < 0.5\%$ across all conditions, indicating that increasing the spatial refinement even more is not required by the selected quantities of interest and flow conditions.

The numerical uncertainty estimation performed in this study focused exclusively on model-scale Reynolds numbers, with and without transition modelling. Due to computational considerations, the decision was made not to perform a similar analysis for full-scale Reynolds numbers.

Recent publications of benchmark cases at full-scale Reynolds numbers indicate a less pronounced sensitivity of the turbulence models on the estimated numerical uncertainties (Eça et al. 2023a, 2023b).

3.2 Transitional flow

As stated in the introduction, transition models exhibit high sensitivity to turbulence quantities within the flow field. The reason is that within the transport equations that are being solved, empirical correlations are calculated that use local quantities. An example is the turbulence intensity Tu which is used in the transition onset momentum-thickness Reynolds number. These local turbulence quantities originate from the inflow boundary conditions and are influenced by the settings used to control the turbulence decay. The substantial comparison error observed for the LCTM γ-Re_θ model as found in previous studies highlighted in the introduction, points towards a strong reliance on local turbulence quantities, especially at design conditions where frictional losses are more pronounced.

This raises a crucial question regarding the selection of inlet values when applying the LCTM transition model. This consideration becomes particularly significant due to the pronounced decay in turbulence quantities by the underlying k-ω SST turbulence model in the case of a uniform flow. As reported by Lopes (2021), the majority of simulations including LCTM transition models use unrealistic high values for the inlet eddy-viscosity ratio in order to reduce the decay of turbulence intensity, but this may also affect the laminar regime. Therefore, a different approach was adopted such that the transport equations for k and ω are solved without the dissipation terms (Lopes et al. 2022). This controlled decay of turbulence quantities acts as a 'frozen' region, extending from the inlet to a specific point in front of the propeller.

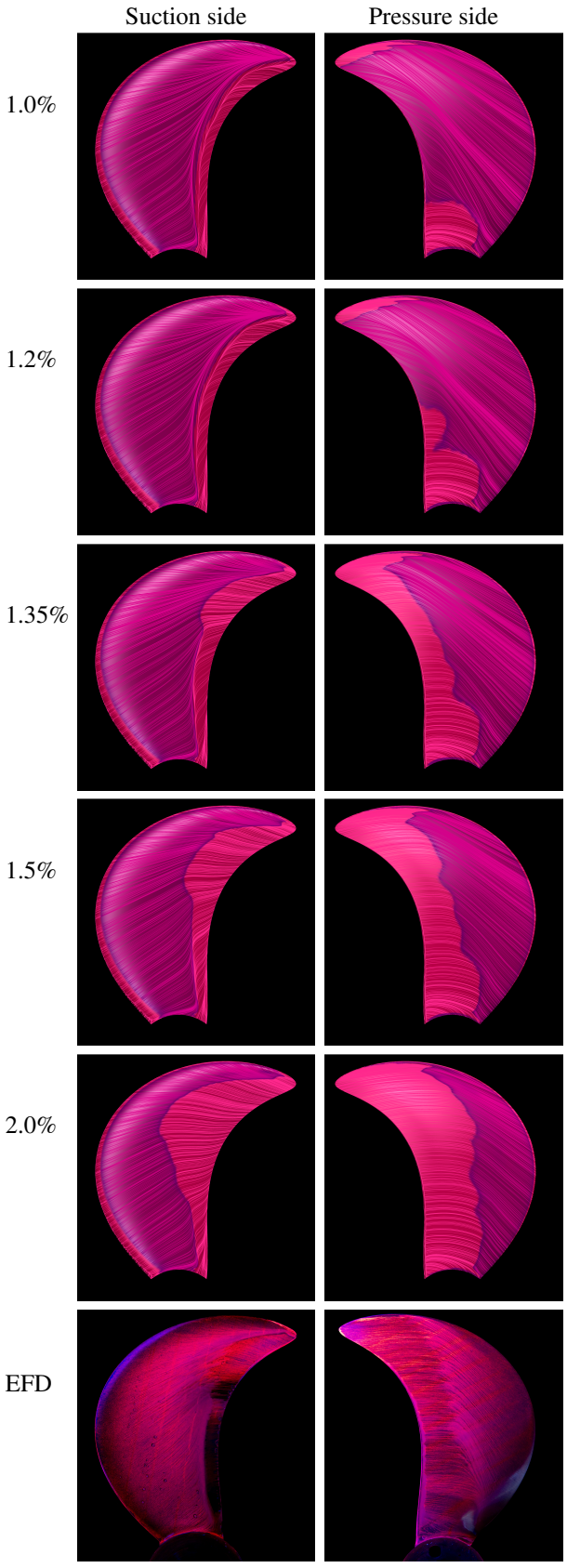

Figure 4: Limiting streamlines and intermittency gradient (contour) on the suction and pressure sides for different inlet turbulence quantities of the LCTM model for $J = 0.8$ at 800 rpm. The bottom row shows paint-test results (EFD) for the same open-water condition ($Re = 7 \cdot 10^5$)

Based on experience from previous studies, e.g. by Baltazar et al. (2023), this decay control ends at a distance equivalent to half the propeller's diameter from the propeller plane. Addressing this involves the analysis of the sensitivity of the flow conditions at the inlet, ensuring agreement of the results with open-water experiments. In order to facilitate a comprehensive comparison that includes not only open-water performance characteristics, but also the boundary layer flow regime, paint test experiments were conducted at MARIN. The methodology for visualizing the boundary layer condition is described in detail by Schuiling et al. (2024).

To mimic the same from the CFD simulations, one of the options to identify and visualise the laminar, transitional, and turbulent boundary-layer regime is to plot the limiting streamlines like the paint streaks from paint-tests. The transition location itself can be detected from the change in the orientation of the limiting streamlines due to the strong increase of local skin-friction. However, this change is often not very abrupt and therefore the intermittency of the transition model is used as well. The intermittency is constrained by a lower limit of 0.02, which is sufficiently small to minimize the generation of turbulence kinetic energy and maintain the laminar state of the boundary layer. If transition occurs, the intermittency rapidly rises to one. Therefore, the magnitude of the intermittency gradient serves as a reliable indicator for identifying the onset of transition.

The results for the design condition at 800 rpm are presented in Figure 4. In these simulations, the turbulence intensity (Tu) of the inflow boundary condition is altered, ranging from 1% to 2%, together with a constant value for the eddy-viscosity ratio of $\mu_t/\mu = 25$. The option to control the decay of the turbulence quantities is activated.

The dark contour colour signifies the presence of laminar flow starting from the leading edge, while the change in contour indicated boundary layer transition or laminar separation. In case of transition the highlighted limiting streamlines shift from a radially directed flow towards a more circumferentially directed flow. In case of laminar separation a distinct detachment line is observed.

Clearly visible from the top figures to the bottom is the alteration of the laminar boundary layer regime due to the increased turbulence intensity. At $Tu = 1\%$ and $Tu = 1.2\%$, the boundary layer state predominantly remains laminar on both the suction and pressure sides, with only a slight initiation of transition observed on the pressure side for lower radii, due to laminar flow separation. In the next stage, $Tu = 1.35\%$, the suction side exhibits transition near 70% of the chord for radii $r/R > 0.7$, while laminar flow separation persists for radii $r/R < 0.7$. On the pressure side, there is an expansion of the region with turbulent flow. Hence, the transition to turbulence is observed at approximately 70% of the chord length and extends evenly across the entire trailing edge. The enlargement of areas featuring turbulent flow continues into the final stage at $Tu = 2.0\%$ and is expected to expand further with continued increases in turbulence intensity. This directly indicates the sensitivity of modern transition models in general and the difficulties in determining boundary conditions and turbulence decay control. Through a visual comparison, it becomes evident that the EFD paint-test results align most closely with the CFD results obtained at a turbulence intensity of 1.35%.

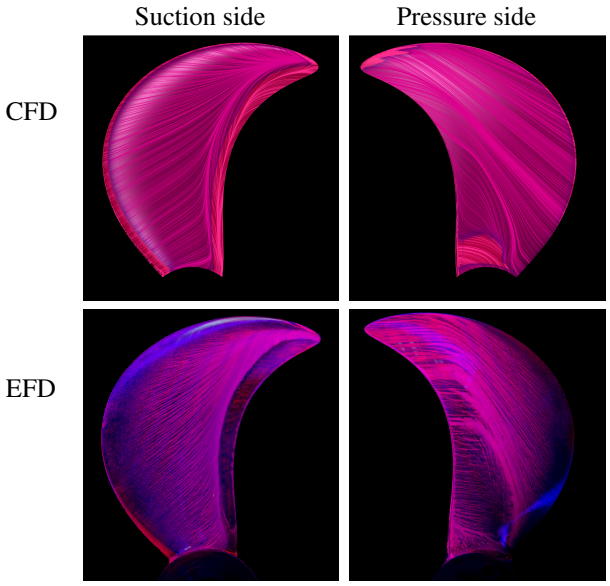

Figure 5: Limiting streamlines and intermittency gradient (contour) on the suction and pressure of the LCTM model for $J = 0.8$ at 400 rpm, compared to paint-test results for the same open-water condition ($Re = 3.5 \cdot 10^5$)

Similar settings for turbulence inflow conditions were employed for the low model-scale Reynolds number. A visual comparison of the limiting streamlines for this condition is presented in Figure 5. The experimental paint-test results reveal a substantial area of laminar flow separation. This characteristic is similarly observed in the corresponding CFD simulations.

3.3 Fully turbulent flow

In light of the drawbacks associated with using the transition modelling, as discussed in the previous section, turbulence models such as the k-ω SST already exhibit high reliability in solving turbulent flows, characterized by minimal sensitivity to boundary conditions. It is for example well known that the k-ω SST turbulence model predicts transition at low Reynolds numbers in the order of 10^4 (Eça and Hoekstra, 2008). Therefore, comparisons with EFD lead to the need to efficiently implement turbulence stimulation on the propeller blades in model testing. Fortunately, this is now possible by using an innovative method proposed by Schuiling et al. (2024), which is inspired by the zigzag strip concept and is characterized by minimal additional drag and enhanced repeatability in testing.

Default settings are applied for the k-ω SST, which means an inflow turbulence intensity $Tu = 1\%$, an eddy-viscosity ratio $\mu_t/\mu = 1$, and no necessity for controlling turbulence decay from the inlet. The CFD results at design condition for the low and high model-scale Reynolds numbers are compared to the same EFD conditions including turbu-

lence stimulation in the experiments. These are illustrated in Figure 6 and Figure 7.

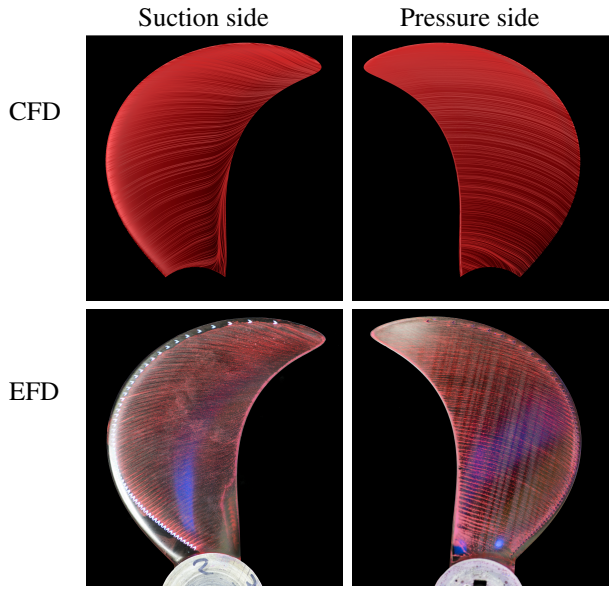

Figure 6: Limiting streamlines on the suction and pressure side with the SST model for $J = 0.8$ at 400 rpm, compared to paint-test results for the same open-water condition ($Re = 3.5 \cdot 10^5$)

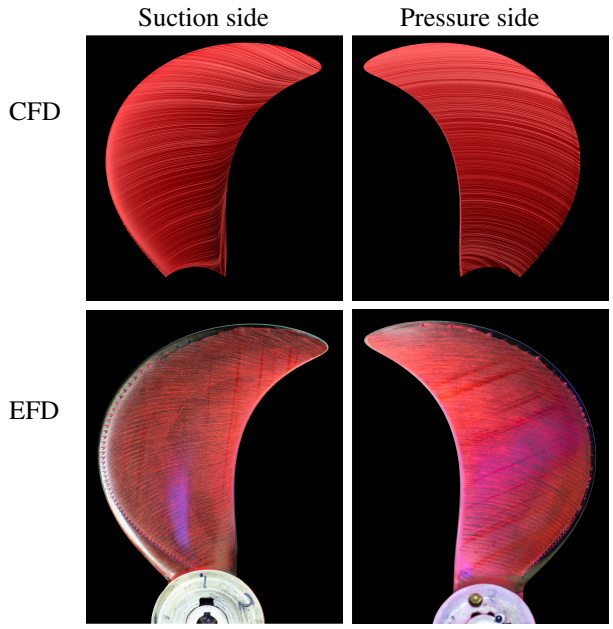

Figure 7: Limiting streamlines on the suction and pressure side with the SST model for $J = 0.8$ at 800 rpm, compared to paint-test results for the same open-water condition ($Re = 7 \cdot 10^5$)

The CFD results reveal a boundary layer that is predominantly turbulent on both the suction and pressure sides. There is only a relatively small region of flow separation near the trailing edge for low radii ($r/R < 0.4$), which is attributed to the adverse pressure gradient in this area. This region is significantly smaller than that observed in simulations which include transition modelling.

The EFD results, including the turbulators at the leading edge, also clearly show a change of the paint patterns, which demonstrate successful tripping of the boundary layer on both the suction and pressure sides.

The positioning of the turbulators down the chord at the lower radii is especially beneficial for propellers with a high thickness-to-chord ratio near the hub. This ensures that the turbulators are not located in the stagnation region and therefore maintain their effectiveness in tripping the laminar boundary layer. An example showing this is presented in Schuiling et al. (2024).

3.4 Open-water characteristics

With a high level of confidence regarding the boundary layer regime over the propeller blade for both transition and turbulent test conditions, the performance characteristics for both model-scale Reynolds conditions are illustrated by the open-water diagram in Figure 8. The upper figure illustrates the low model-scale Reynolds number, while the lower figure depicts the high model-scale Reynolds number. The design condition $J = 0.8$ is indicated by the vertical dashed line.

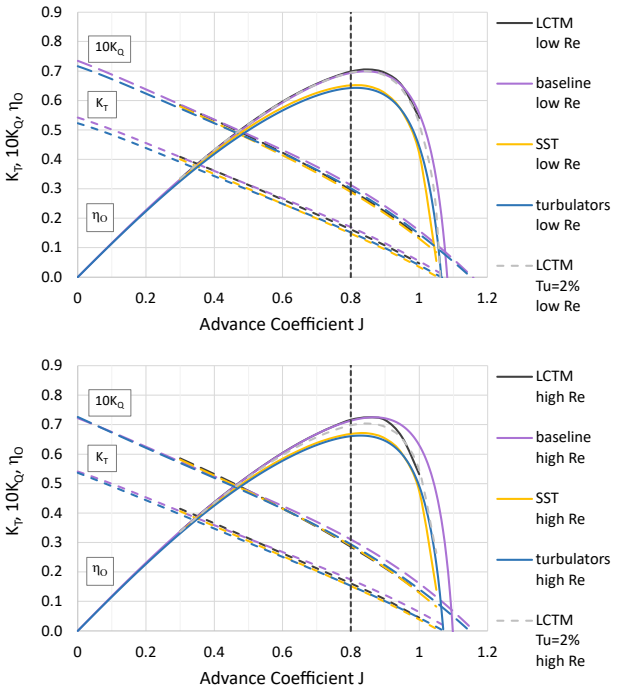

Figure 8: Open-water diagram for 400 rpm (top) and 800 rpm (bottom). The lines show CFD results for both the LCTM and SST model, and the EFD results with and without turbulators

The first observation to be made is that the agreement level for identical boundary layer regimes is significantly higher than the difference observed between distinct boundary layer regimes. The comparison between the LCTM γ-Re_θ transition model (displayed in black) and the k-ω SST turbulence model (displayed in yellow), shows an absolute difference $\Delta\eta_o$ of about 5% at the design condition. Also

the relative thrust coefficient K_T differs with values from 6% to 10%, similar to the observations from the experiments (Schuiling et al. 2024). Comparatively smaller discrepancies are found in the comparison between identical boundary layer regimes. The results from the baseline propeller EFD without turbulators (displayed in purple) shows good agreement with the CFD results that include the LCTM transition model (displayed in black). To provide a comprehensive view, the results of the open-water efficiency with a slightly increased turbulence intensity ($Tu = 2\%$) are also presented (represented by the dashed grey lines).

In general the comparison difference in open-water efficiency between the LCTM results ($Tu = 1.35\%$) with the EFD results is minimal. At the design condition $J = 0.8$ an absolute difference $\Delta\eta_o$ is found of 0.35% for 800 rpm and 0.45% for 400 rpm. The relative difference in the complete advance range $0 < J < 0.8$ is less than 0.6%, for both Reynolds numbers. Additionally, the relative comparison difference for K_T and K_Q at the advance coefficients $0.3 < J < 0.6$ is less than 2%, reaching a maximum value of approximately 6% around the design condition. Furthermore, the results of the increased turbulence intensity $Tu = 2\%$ with respect to $Tu = 1.35\%$ primarily leads to a decrease of K_T ranging from 1% to 3%, especially for the high model-scale Reynolds number, while K_Q remains relatively consistent. At the design condition $J = 0.8$, this results in an absolute efficiency decrease of 1.8% for 800 rpm, whereas there is only a minor change of 0.3% for 400 rpm.

Moreover, the CFD results with the SST turbulence model (displayed in yellow) demonstrate an even better correspondence with EFD results of the propeller including turbulators near the leading edge (displayed in blue). The absolute comparison difference in open-water efficiency η_o is approximately 1% over the complete advance coefficient range and the relative comparison difference for K_T and K_Q is smaller than 3%. This level of agreement highlights the reliability and accuracy of the CFD simulations in capturing the turbulent flow conditions, thereby strengthening the overall agreement of CFD with the experimental data.

3.5 Flow details

Numerical methods present a substantial advantage compared to experiments, as they enable a more straightforward and detailed examination of flow characteristics. To understand how the boundary layer regime affects the resulting thrust and torque, a visual representation of the contributions of pressure and wall shear stress to these results is generated and analysed, with particular attention to the variations arising from differences in boundary layer status.

The individual contribution of dimensionless force (C_F) and moment (C_M) of skin-friction (f) and pressure (p) on propeller thrust and torque is calculated as follows:

$$\begin{aligned} \vec{C}_{F_f} &= \frac{\vec{\tau}_w}{1/2\rho V_{\text{ref}}^2} \\ \vec{C}_{F_p} &= \frac{p \cdot \vec{n}_f}{1/2\rho V_{\text{ref}}^2} \end{aligned} \tag{13}$$

$$\begin{aligned} \vec{C}_{M_f} &= \frac{\vec{\tau}_w \times \vec{r}}{1/2\rho V_{\text{ref}}^2 R} \\ \vec{C}_{M_p} &= \frac{(p \cdot \vec{n}_f) \times \vec{r}}{1/2\rho V_{\text{ref}}^2 R} \end{aligned} \tag{14}$$

With for each boundary face, p the local pressure, $\vec{\tau}_w$ the local wall shear stress vector, $\vec{n}_f$ surface normal vector and $\vec{r}$ the position vector with respect to the origin.

The skin-friction contribution, acting as a negative thrust, is visualised in Figure 9 by the component of skin-friction directed in the axial direction (x), therefore indicated as $C_{F_{f,x}}$. Due to the fully turbulent nature of the boundary layer in the SST results, there is a strong increase in frictional resistance in contrast to the laminar boundary layer observed in the LCTM results. The effect is particularly pronounced at higher radii, where local velocity increases. Positive values in the regions near the trailing edge indicate the presence of boundary layer flow separation that does not re-attach.

The contribution of the pressure, acting as positive thrust, is also visualised in Figure 9 showing only the axial directed part indicated by $C_{F_{p,x}}$. The surface distribution is highly comparable between both CFD results, but the SST results show slightly lower positive levels, leading to an overall decrease in thrust. This can be explained by the turbulent nature of the boundary-layer that leads to a significant increase of the displacement thickness when compared to the laminar case. As a consequence, the effect of the boundary-layer on the curvature of the outer flow streamlines is more pronounced for the turbulent flow, which justifies the changes of the pressure on the blade surface and thus a decrease of the generated thrust.

This analysis is also extended to examine the contributions of skin-friction and pressure on the resulting required torque, which is visualised in Figure 9, indicated as $C_{M_{f,x}}$ and $C_{M_{p,x}}$, respectively. Positive values indicate an increase in required torque, whereas a negative value reduces the required torque. Again, the increased skin-friction resulting from the turbulent nature of the boundary layer is clearly evident in the SST results, thereby increasing the torque. But conversely, when comparing the LCTM results for the pressure contribution, it reveals a higher required torque for laminar flow. This counteracting effect due to the flow regime of the boundary layer creates great uncertainty when the transition location shifts or flow separation occurs.

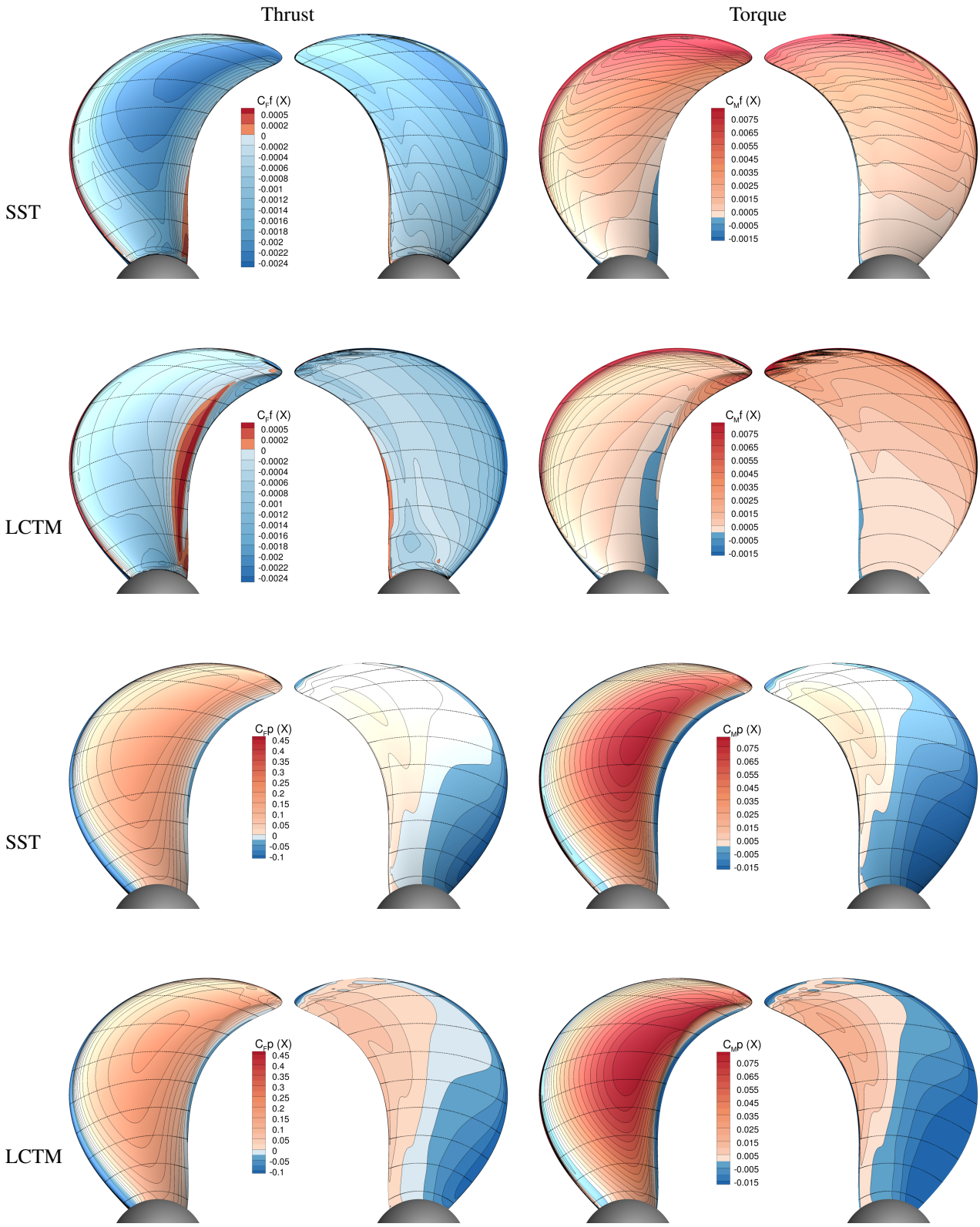

Figure 9: Surface distribution of the individual contribution of skin-friction and pressure on total thrust for the design condition $J = 0.8$ at 400 rpm ($Re = 3.5 \cdot 10^5$)

Figure 10 illustrates the local differences between the two models, being $\Delta = \text{SST} - \text{LCTM}$. In the upper figure, the blue regions highlight areas predominantly influenced by the laminar boundary layer and flow separation in the LCTM simulation. Notice a substantial region on the suction side, including the flow separation near the trailing edge, which is in favour of the resulting thrust.

Conversely, the extensive flow separation region results in an increase of torque for the LCTM solution, as depicted in the lower figure. This is due to an increase of sectional pressure drag due to flow separation. On the other hand, the effect of the turbulent boundary layer contributes to an increase of torque for SST. This underlines the difficulty in managing cancelling terms that are both hard to anticipate and challenging to incorporate into an extrapolation process for predicting full-scale performance. This challenge is particularly pronounced when these terms exhibit high sensitivity to the operating regime of the boundary layer, as is the case with transitional flows.

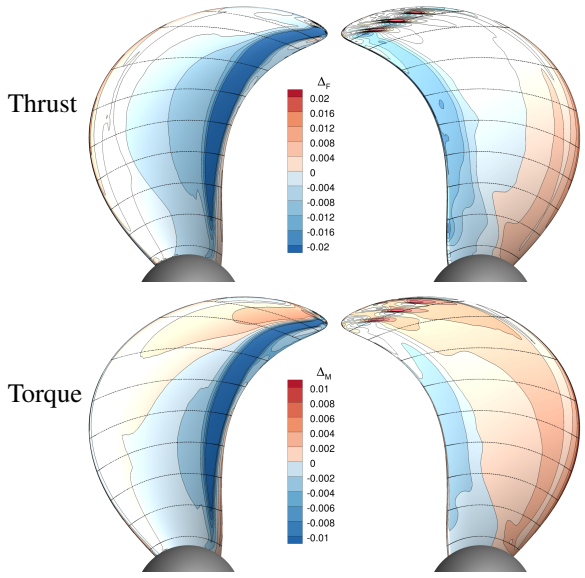

Figure 10: Surface distribution of the difference between the obtained SST minus LCTM results for the design condition $J = 0.8$ at 400 rpm ($Re = 3.5 \cdot 10^5$)

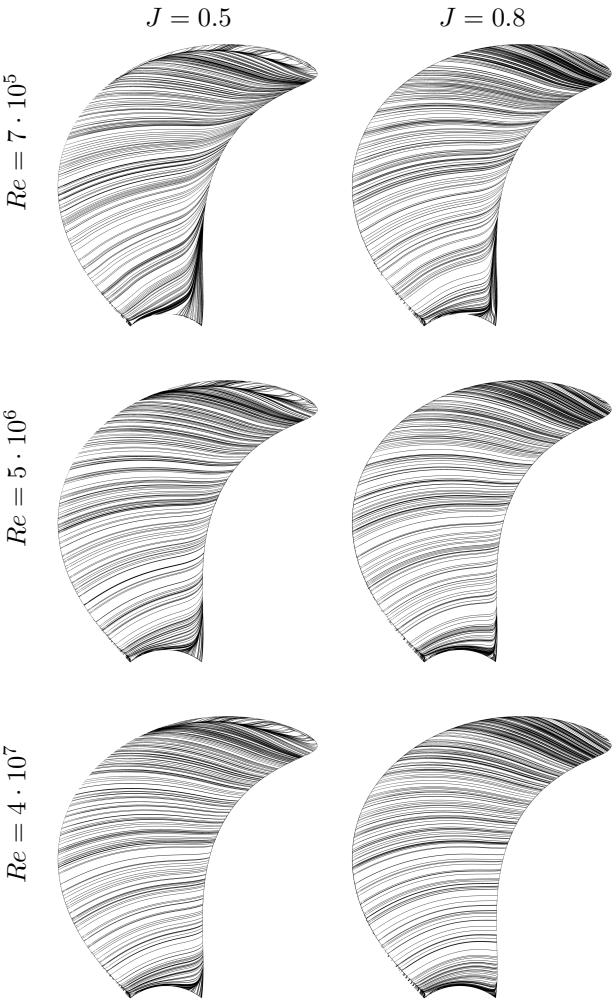

Figure 11: Limiting streamlines of the flow on the suction side of the propeller at $J = 0.5$ (left) and $J = 0.8$ (right) for different Reynolds numbers

Table 4: Propeller conditions for full-scale CFD simulations based on the geometrical scale-factor $\lambda = 35$

Propeller Conditions		Reynolds Numbers			
	Re [-]	$5 \cdot 10^6$	$1 \cdot 10^7$	$4 \cdot 10^7$	$8 \cdot 10^7$
J=0.8	V_S [knots]	1.3	2.5	10	20
	n [rpm]	4.7	9.3	36.7	73.5

3.6 Full-scale propeller performance

Simulations are conducted for full-scale Reynolds numbers, ranging from $5 \cdot 10^6$ to $8 \cdot 10^7$. The conditions are established using a scale factor $\lambda = 35$, and the associated full-scale advance velocity and propeller rotation rate are provided by Table 4. Like the model-scale simulations, default settings are applied for the k-ω SST, which in this case are an inflow turbulence intensity $Tu = 5\%$ and an eddy-viscosity ratio $\mu_t/\mu = 10$. The grid is further refined in the normal direction to the wall, such that for the near-wall cells $y^+ < 1$ for all Reynolds numbers. This means that the boundary layer is fully resolved without wall-functions.

In Figure 11 the limiting streamlines of the flow on suction side of the propeller are presented for three Reynolds numbers at $J = 0.5$ and design condition $J = 0.8$. From the figures it can be concluded that with an increase in Reynolds number the limiting streamlines become more circumferentially directed, due to the higher shear-stress component. The difference is most pronounced near the trailing edge. Additionally, the small regions with existing flow separation at the lower radii near the trailing edge disappear with the increase of the Reynolds number. Apart from these minor visual differences in the behaviour of the turbulent boundary layer, there are no other distinctions in

the boundary layer regime observed between the model and the full-scale Reynolds numbers.

The full-scale performance results are presented by the open-water diagram in Figure 12. Scaling from model-scale Reynolds numbers (displayed in black) to an increasing Reynolds number at full-scale (displayed in purple, yellow, blue, and green) primarily affects the thrust coefficients, while the torque coefficients experience minimal change. Hence, an increase in the Reynolds number leads to an overall improvement in open-water efficiency. This phenomenon is illustrated by Figure 13 for the results at the design condition $J = 0.8$. The picture depicts the variation of the quantities of interest with respect to the fully turbulent model-scale results at 800 rpm ($Re = 7 \cdot 10^5$). Both the thrust coefficient K_T and propeller efficiency η_o show an increase up to 10% and 6.4%, respectively, whereas the changes in torque coefficient K_Q are smaller than 0.4%.

These conclusions are in contrast to the trends observed for the model-scale experimental and simulation results that account for transitional effects. Those results showed a pronounced shift in torque coefficient due to changes of the boundary layer regime that are strongly dependent on the evaluated Reynolds condition. Also, this significant effect on the thrust coefficient is not included when extrapolating model-scale results to full-scale predictions using the ITTC 1978 Propeller Performance Prediction Method. This is illustrated by the extrapolated open-water performance predictions in Figure 12. Here, the standard ITTC 1978 propeller extrapolation formulas are applied to the model-scale results at 800 rpm, based on the fully turbulent SST (displayed in grey) and the laminar-turbulent transition LCTM simulations (displayed in red). Both results show an increase in thrust coefficient and efficiency but also a decrease in torque coefficient. It is important to note that the current CFD simulations do not account for the effects of blade surface roughness, as they do for the extrapolated values within the ITTC procedure.

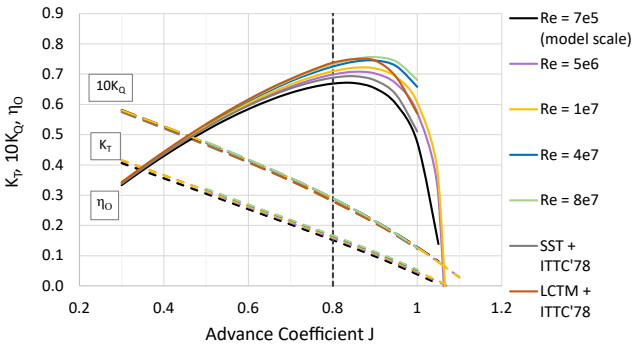

Figure 12: Open-water diagram for a range of Reynolds numbers and extrapolated performance prediction based on the ITTC'78 procedure

The comparison at design condition $J = 0.8$ is illustrated in Figure 13. The relative increase of the thrust coefficient ΔK_T due to the extrapolation method is approximately 0.6%, whereas the torque coefficient ΔK_Q exhibits a reduction of 2.3%. This results in an absolute increase of the open-water efficiency of only 2.0%, as displayed in grey. The same applies to the LCTM results, leading to an absolute efficiency difference of 6.9% compared to the fully turbulent SST model-scale results, as displayed in red. This distinctly highlights the significantly larger scaling impact of the extrapolation method on K_Q compared to K_T, in contrast to the earlier observed trend across a range of full-scale Reynolds numbers.

As illustrated in this paper, the laminar boundary layer observed at model-scale tends to separate under adverse pressure gradients, leading to flow separation near the trailing edge of the propeller. Additionally, a shift in the onset of the laminar boundary layer transition is observed for different Reynolds numbers. These aspects are tough to realise in Reynolds scaling procedures, prompting the question of the practicality of scaling these effects, especially given their sensitivity to propeller design. Fortunately, both issues are mitigated by introducing a turbulent boundary layer at model-scale, resulting in attached flow, mirroring the behaviour observed at full-scale conditions. Therefore, it is required to further research the potential development of a propeller performance extrapolation methodology, based on Reynolds scaling and derived from thorough model and full-scale CFD simulations. This improves the uncertainty of full-scale propeller performance predictions when the extrapolation procedure is applied to model-scale experiments where the propeller, equipped with turbulators, encounters a turbulence boundary layer at the model-scale Reynolds number.

4 CONCLUSIONS

This study offers insights into the application of a turbulence model with or without transition model for open-water propeller simulations, in comparison to experimental results including visualization of the flow through paint-tests. From the results, it can be concluded that it is possible to accurately predict the performance of an open-water propeller at model-scale, including the effect of transition and flow separation, using the LCTM γ-Re_θ transition model. However, small discrepancies between experiments and simulations can only be achieved if the onset of transition and possible flow separation is known *a priori*. The assessment of the physical boundary layer regime is evaluated by experimental paint tests that clearly indicate the occurrences of transition and flow separation. These findings are compared with numerical skin-friction flow lines. The onset of transition, predicted by the LCTM γ-Re_θ model, highly depends on the inflow boundary condition and the decay of turbulence. Tuning these boundary conditions and utilizing a turbulence decay control method is highly recommended. Nevertheless, given the presence of these uncertainties of the boundary layer regime in transitional flows, it becomes questionable whether an accurate prediction of the propeller performance from such a model-scale problem to full-scale is possible.

Therefore a feasible alternative is demonstrated, since the CFD results performed with the k-ω SST turbulence model provide a very good comparison with the open-water ex-

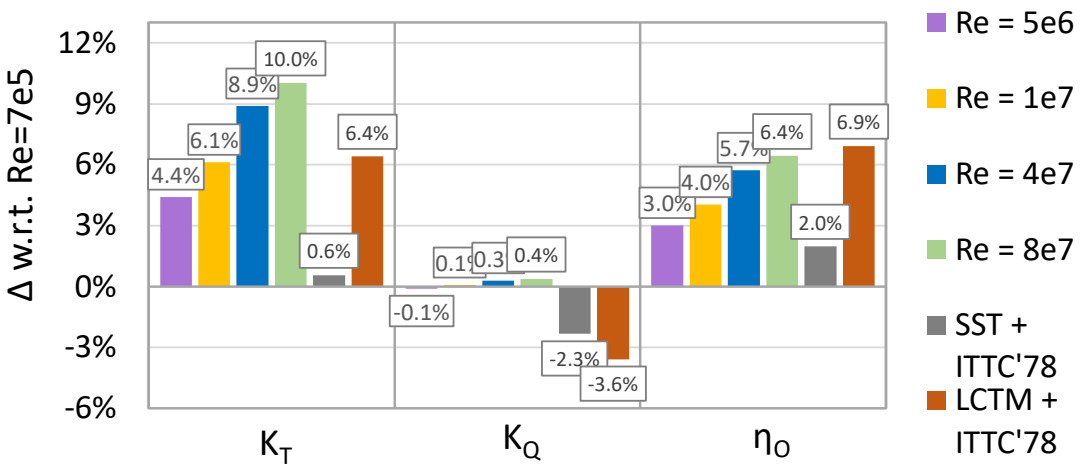

Figure 13: Reynolds scaling effect on the propeller performance at design condition $J = 0.8$ with respect to the model-scale Reynolds number ($Re = 7 \cdot 10^5$)

periments. These experiments were performed with turbulators at the leading edge to trip the boundary layer in a controlled manner. The discrepancy between experiments and simulations (comparison error) in open-water efficiency η_o is approximately 1% and the comparison errors for K_T and K_Q are smaller than 3%. The numerical uncertainties, as determined through a grid refinement study, were found to be smaller than the comparison errors, with $U < 0.5\%$ across all conditions. This indicates a high level of confidence in the results of the simulations.

The conclusions drawn from the results of the Reynolds number range, from model to full-scale, indicate that there are only slight differences in the boundary layer regime. Reynolds scaling primarily impacts on the thrust coefficients, up to 10%, while the torque coefficients experience minimal change, smaller than 0.5%. Hence, an increase in the Reynolds number leads to an overall improvement in open-water efficiency η_o up to 6%.

The difference between model and full-scale results, due to Reynolds scaling, requires further investigation. This research should explore the feasibility of developing a new propeller performance extrapolation procedure from extensive model and full-scale CFD simulations, enabling its application in model-scale experiments where the propeller, equipped with turbulators, exhibits a turbulence boundary layer at the model-scale Reynolds number.

In this study, the primary emphasis was placed on the design condition, as the relative impact of viscous losses is most pronounced under these circumstances. Furthermore, the propeller efficiency at design condition is usually the most important measure of the propeller performance for propulsion prediction.

In conclusion, this research enhances the understanding of boundary layer behaviour in model and full-scale propellers. These insights are essential for improving model-test accuracy and to enhance the accuracy of full-scale performance predictions, with as end goal to design more efficient marine propulsion systems.

Acknowledgements This research was partly funded by the Dutch Ministry of Economic Affairs. Additionally, we express our gratitude to Jeroen Reus M.Sc. for his outstanding work during his internship.

REFERENCES

Allan, J.F., Couch, R.B., Lerbs, H.W.E., Telfer, E.V. (1951). 'Subject 1 - Reynolds Number for Model Propeller Experiments'. 6th International Conference of Ship Tank Superintendents, ITTC, Washington, United States of America.

ASME V&V20. (2009). 'Standard for Verification and Validation in Computational Fluid Dynamics and Heat Transfer'. American Society of Mechanical Engineers.

Aucher, M., Bowden, B.S., Gross, A., Lindgren, H., Minsaas, K.J., Muntjewerf, J.J., Tamura, K., Wermter, R. (1978). 'Report of Performance Committee'. 15th International Towing Tank Conference, ITTC, The Hague, The Netherlands.

Baltazar, J., Rijpkema, D. & Falcão de Campos, J. (2018). 'On the use of the γ-Re_{θ_t} transition model for the prediction of the propeller performance at model-scale'. Ocean Engineering, **170**:6-19.

Baltazar, J., Rijpkema, D. & Falcão de Campos, J. (2021). 'Prediction of the Propeller Performance at Different Reynolds Number Regimes with RANS'. Journal of Marine Science and Engineering, **9**(10):1115.

Baltazar, J., Schuiling, B. & Kerkvliet, M. (2023). 'Modelling of Laminar-to-Turbulent Flow Transition on a Marine Propeller Using a RANS Solver'. 25th Numerical Towing Tank Symposium, NuTTS'23, Ericeira, Portugal.

Boorsma, A. (2000). 'Improving full scale ship powering performance predictions by application of propeller leading edge roughness'. MSc Thesis, Delft University of Technology, Delft, The Netherlands.

Eça, L. & Hoekstra, M. (2008). 'The numerical friction line'. Journal of Marine Science and Technology, **13**:328-345.

Eça, L. & Hoekstra, M. (2014). 'A procedure for the estimation of the numerical uncertainty of CFD calculations based on grid refinement studies'. Journal of Computational Physics, **262**:104-130.

Eça, L., Kerkvliet, M. & Toxopeus, S.L. (2023a). 'Comparison of RANS Turbulence Models for the Simulation of Smooth Wall Boundary-Layers in Pressure Gradients at Moderate and High Reynolds Numbers'. 10th International Conference on Computational Methods in Marine Engineering, MARINE, Madrid, Spain.

Eça, L., Kerkvliet, M. & Toxopeus, S.L. (2023b). 'Using Validation Metrics to Assess RANS Turbulence Models Performance at Full Scale Reynolds Numbers'. Proceedings of International Mechanical Engineering Congress & Exposition, IMECE, New Orleans, LA, USA.

Eça, L., Toxopeus, S.L. & Kerkvliet, M. (2023c). 'Procedures for the Estimation of Numerical Uncertainties in the Simulation of Steady and Unsteady Flows'. Technical Report IST-M 8, Universidade de Lisboa - Instituto Superior Tecnico , Lisbon, Portugal.

Fagerjord P. & Andersen K. (1982). 'Are the Existing Methods to Obtain Maximum Propulsion Efficiency Appropriate'. Symposium on Ship Costs and Energy, SNAME.

Gaggero, S. (2022). 'Influence of laminar-to-turbulent transition on model scale propeller performances. Part I: fully wetted conditions'. Ships and Offshore Structures, **17**(4), 715-727.

Grlj, C.G., Degiuli, N., Farkas, A. & Martić, I. (2022). 'Numerical Study of Scale Effects on Open Water Propeller Performance'. Journal of Marine Science and Engineering, **10**(8):1132.

Hasuike, N., Okazaki, M., Okazaki, A. & Fujiyama, K. (2017). 'Scale effects of marine propellers in POT and self propulsion test conditions'. Proceedings of the Fifth International Symposium on Marine Propulsors, SMP'17, Espoo, Finland.

ITTC (2014). 'Testing and Extrapolation Methods Propulsion, Propulsor Open Water Test'. Recommended Procedures and Guidelines, 7.5-02-03-02.1

ITTC (2017). '1978 Powering Prediction Method'. Recommended Procedures and Guidelines, 7.5-02-03-01.4

Jessup, S.D. (1989). An experimental investigation of viscous aspects of propeller blade flow. PhD thesis, The Catholic University of America, Washington D.C., USA.

Katsuno, E.T., Lidtke, A.K., Duz, B., Rijpkema, D., Dantas, J.L.D. & Vaz G. (2021). 'Estimating parameter and discretization uncertainties using a laminar–turbulent transition model'. Computers and Fluids, **230**:105129.

Kuiper, G. (1981). Cavitation inception on ship propeller models. PhD thesis, Delft University of Technology, Delft, Netherlands.

Langtry, R. & Menter, F. (2009). 'Correlation-based transition modeling for unstructured parallelized computational fluid dynamics codes'. AIAA Journal, **47**(12), 2894–2906.

Li, D.-Q., Lindell, P. & Werner, S. (2019). 'Transitional Flow on Model Propellers and Their Influence on Relative Rotative Efficiency'. Journal of Marine Science and Engineering, **7**(12):427.

Lopes, R. (2021). Simulation of Transition from Laminar to Turbulent Regime in Practical Applications of Incompressible Flow. PhD thesis, Universidade de Lisboa - Instituto Superior Tecnico , Lisbon, Portugal.

Lopes, R., Eça, L., Vaz, G. & Kerkvliet, M. (2022). 'A Technique to Control the Decay of Freestream Turbulence for Transitional Flow Simulations'. AIAA Journal, **60**(6):3565–3580.

Lopes, R., Eslamdoost, A., Johansson, R., Roychoudhury, S. & Bensow, R.E. (2023). 'Crossflow transition modelling for a marine propeller at model scale'. 25th Numerical Towing Tank Symposium, NuTTS'23, Ericeira, Portugal.

Lücke, T (2019). 'Particular Model Propeller Behavior in EFD & CFD'. Proceedings of the Sixth International Symposium on Marine Propulsors, SMP'19, Rome, Italy.

Moran-Guerrero, A., Gonzalez-Gutierrez, L.M., Oliva-Remola, A. & Diaz-Ojeda, H.R. (2018). 'On the influence of transition modeling and crossflow effects on open water propeller simulations'. Ocean Engineering, **156**:101-119.

Menter, F., Kuntz, M. & Langtry, R. (2003). 'Ten years of industrial experience with the SST turbulence model'. Proceedings of the Fourth International Symposium of Turbulence, Heat and Mass Transfer, Antalya, Turkey.

Rijpkema, D., Baltazar, J. & Falcão de Campos, J. (2015). 'Viscous flow simulations of propellers in different Reynolds number regimes'. Proceedings of the Fourth International Symposium on Marine Propulsors, SMP'15, Austin, Texas, USA.

Schuiling, B., Kerkvliet, M. & Rijpkema, D. (2024). 'An Experimental Study on Flow Visualisation and Passive Control of Model Propeller Boundary Layers'. Proceedings of the Eighth International Symposium on Marine Propulsors, SMP'24, Berlin, Germany.

Tamura, K. & Sasajima, T. (1977). 'Some Investigations on Propeller Open-Water Characteristics for Analysis of Self-Propulsion Factors'. Mitsubishi Technical Bulletin **66**, Mitsubishi Heavy Industries Ltd., Tokyo, Japan.